Enhanced Conductivity *via* Homopolymer-Rich Pathways in Block Polymer Blended Electrolytes

Melody A. Morris,[a] Seung Hyun Sung,[a] Priyanka M. Ketkar,[a] Joseph A. Dura,[b] Ryan C. Nieuwendaal,[c] and Thomas H. Epps, III[a,d,]*

[a]Department of Chemical & Biomolecular Engineering, University of Delaware, Newark, DE 19716, United States

[b]NIST Center for Neutron Research, National Institute of Standards and Technology, Gaithersburg, MD 20899, United States

[c]Materials Science and Engineering Division, National Institute of Standards and Technology, Gaithersburg, MD 20899, United States

[d]Department of Materials Science and Engineering, University of Delaware, Newark, DE 19716, United States

ABSTRACT

The optimization of ionic conductivity and lithium-ion battery stability can be achieved by independently tuning the ion transport and mechanical robustness of block polymer (BP) electrolytes. However, the ionic conductivity of BP electrolytes is inherently limited by the covalent attachment of the ionically-conductive block to the mechanically-robust block, among other factors. Herein, the BP electrolyte polystyrene-*block*-poly(*oligo*-oxyethylene methacrylate) [PS-*b*-POEM] was blended with POEM homopolymers of varying molecular weights. The incorporation of a higher molecular weight homopolymer additive ($\alpha > 1$ state) promoted a 'dry brush-like' homopolymer distribution within the BP self-assembly and led to higher lithium salt concentrations in the more mobile homopolymer-rich region, increasing overall ionic conductivity relative to the 'wet brush-like' ($\alpha < 1$ state) and unblended composites, where α is the molecular weight ratio between the POEM homopolymer and the POEM block in the copolymer. Neutron and X-ray reflectometry (NR and XRR, respectively) provided additional details on the lithium salt and polymer distributions. From XRR, the $\alpha > 1$ blends showed increased interfacial widths in comparison to their BP (unblended) or $\alpha < 1$ counterparts because of the more central distribution of the homopolymer. This result, paired with NR data that suggested even salt concentrations across the POEM domains, implied that there was a higher salt concentration in the homopolymer POEM-rich regions in the dry brush blend than in the wet brush blend. Furthermore, using ^{7}Li solid-state nuclear magnetic resonance spectroscopy, we found a temperature corresponding to a transition in lithium mobility ($T_{Li\ mobility}$) that was a function of blend-type. $T_{Li\ mobility}$ was found to be 39 °C above T_g in all cases. Interestingly, the ionic conductivity of the blended BPs was highest in the $\alpha > 1$ composites even though these composites had higher T_gs than the $\alpha < 1$ composites, demonstrating that homopolymer-rich conducting pathways formed in

the $\alpha > 1$ assemblies had a larger influence on conductivity than the greater lithium ion mobility in the $\alpha < 1$ blends.

For Table of Contents Use Only

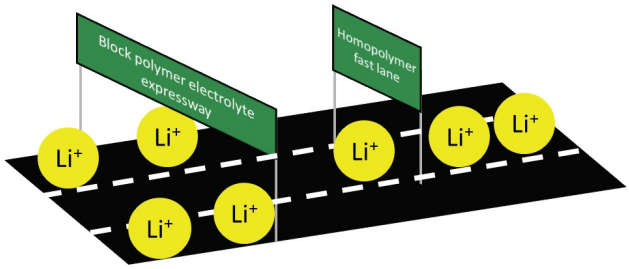

Enhanced Conductivity *via* Homopolymer-Rich Pathways in Block Polymer Blended Electrolytes

Melody A. Morris, Seung Hyun Sung, Priyanka M. Ketkar, Joseph A. Dura, Ryan C. Nieuwendaal, and Thomas H. Epps, III

INTRODUCTION

Lithium-ion batteries are some of the most widely-used energy storage devices because of their high energy densities and their ability to be recharged for hundreds of cycles.[1-2] In most commercial lithium-ion battery systems, the electrolyte is a flammable liquid with a thin polymer membrane as a separator.[3] Because of the lack of overall mechanical robustness combined with the flammability of the liquid electrolyte, current batteries are subject to catastrophic failure as a result of, for example, separator fracture or lithium dendrite penetration.[2-5] To improve the mechanical robustness of the electrolyte and mitigate these issues, replacing the liquid electrolyte/separator system with homopolymer or block polymer (BP) electrolytes has been examined.[6-15] However, an appropriate balance between conductivity and mechanical robustness is required to develop safe and commercializable lithium-ion batteries.[1, 6-7, 16-17]

Because the majority of lithium-ion conductivity in a polymer electrolyte occurs by segmental chain motion of the polymer and inter- and intra-chain hopping of the ions, one method to enhance the lithium-ion mobility is to decrease the glass transition temperature (T_g) of the conducting component of the polymer electrolyte.[5] Homopolymer electrolytes, such as poly(ethylene oxide) [PEO] doped with a lithium salt, have high ionic conductivity, as they are composed of entirely ion-conducting material and are not covalently bound to a less-mobile high-T_g block.[18-19] However, as many homopolymer electrolytes are engineered to have low T_g, their shear modulus is insufficient to prevent mechanical failure.[20-21] BP electrolytes typically consist of ion-conducting polymer covalently attached to a high-T_g block, such as polystyrene (PS).[17, 22-23] In a BP electrolyte, as a result of the phase-separated domains, the ionic conductivity and shear modulus are decoupled, enabling simultaneous optimization of the two properties.[17, 22-24] Nonetheless, the ionic conductivity remains limited in these BP electrolyte systems.[18, 25] Creating

a homopolymer-blended BP electrolyte is a promising strategy to achieve a more desirable balance of ionic conductivity (enhanced by the homopolymer additives) and mechanical robustness (maintained by the BP nanostructure and high-T_g component), though it is essential to understand the role of homopolymer molecular weight and volume fraction on the homopolymer and salt distributions (and ultimately the ion transport) in these composite electrolytes.

Non-salt-doped model systems composed of a homopolymer A blended with a BP A-*b*-B have been examined both theoretically and experimentally to understand the distribution of homopolymer within the BP matrix and the morphology of the resulting system.[26-31] It has been established that the ratio of the homopolymer molecular weight to the molecular weight of the corresponding block in the BP ($\alpha = M_{n,A\ in\ homopolymer}/M_{n,A\ in\ BP}$) and the homopolymer volume fraction in the blend (φ_H) affect the morphology and distribution of homopolymer in the self-assembled, composite system.[26-30] In the limit of high α, the homopolymer forms its own domain, termed "dry brush", whereas in the limit of $\alpha = 0$, the homopolymer has a similar distribution to that of the A block in the BP, termed "wet brush".[26-27, 30] More specifically, from self-consistent field theory, the $\alpha > 1$ case leads to homopolymer distributions, which are dependent only on the brush overlap parameter, w_{OL} (a system-specific parameter), that approach symmetric hyperbolic tangents centered around the middle of the domain.[27] The $\alpha < 1$ case, however, leads to homopolymer distributions that are a function of both the homopolymer molecular weight and w_{OL}, in which the homopolymer tends to distribute more evenly at lower molecular weights.[27] For higher φ_H, both the breadth and the maximum concentration of the homopolymer distribution increases.[26, 31] These theoretically-predicted trends have been verified experimentally in lamellae-forming systems with neutron reflectometry (NR) experiments on PS-*b*-polyisoprene/deuterated PS (PS-*b*-PI/dPS) and PS-*b*-poly(methyl methacrylate)/dPS blends across a variety of α, φ_H, and

$M_{n,BP}$ values.[26, 30] Manipulating the blend characteristics to achieve a desired homopolymer distribution is useful in engineering the next generation of composite systems.

Beyond the homopolymer distribution, Matsen developed phase diagrams for these A-*b*-B/A blends using self-consistent field theory for a variety of values of φ_H and α.[29] Many of the classical phases, such as lamellae and hexagonally-packed cylinders, were found, but phases that are less typical in equilibrated BP systems, such as hexagonally-perforated lamellae, also were noted.[29] Furthermore, blends with homopolymer incorporated at relatively high volume fractions ($\varphi_H = 0.4, f_A = 0.5, \chi N = 12$) maintained a lamellar morphology, which suggests that a large phase window exists for performing reflectometry-based studies.[29] Finally, recent work on homopolymer blends has suggested that the addition of low molecular weight homopolymers promotes rapid annealing of thin films and stabilizes a bicontinuous microemulsion phase (which may have promising ion conducting properties) in the case of ternary A-*b*-B/A/B blends.[32-34] In developing a salt-doped homopolymer-blended BP electrolyte system, parameters like α, φ_H, and the salt-doping ratio, r, can be used to manipulate the combined salt and polymer density profiles such that the lithium salt is doped at ideal concentrations in a given component in the composite electrolyte.

In an A-*b*-B/A blended BP electrolyte system, the distribution of salt also is of interest because the ionic conductivity of an electrolyte is highly dependent on the salt concentration such that there exists a salt concentration that leads to a maximum conductivity. The salt concentration that promotes maximum conductivity depends on the polymer system because of the local stresses in the ion-conducting component.[35] For example, in PEO-based electrolytes doped with lithium bis(trifluoromethane)sulfonimide (LiTFSI), the ionic conductivity is maximized at a salt-doping ratio (molar ratio of ethylene oxide monomer segments in the PEO to lithium ions) of

[EO]:$[Li]_{\sigma,max}$ = 9:1, whereas, in PS-*b*-PEO-based electrolytes doped with the same salt, the maximum conductivity is at [EO]:$[Li]_{\sigma,max}$ = 5:1.[12] Because conductivity is affected by a number of interrelated factors including morphology, alignment, and local salt concentration, it is important to deconvolute these influences using a combination of bulk conductivity and lithium mobility measurements.[35-37] It is anticipated that if the local concentration of salt is controlled such that the most mobile region of a polymer electrolyte is doped at [EO]:$[Li]_{\sigma,max}$, the conductivity of that particular electrolyte would be maximized.

The salt distribution in a salt-doped BP has been elucidated using a variety of techniques, including energy-filtered transmission electron microscopy (EF-TEM),[35] X-ray photoelectron spectroscopy (XPS) with C_{60}^+ etching,[38] and NR.[39] Though there has not been complete agreement between these studies, these differences possibly can be attributed to differences in BPs (PS-*b*-PEO in the EF-TEM studies *vs.* PS-*b*-poly(*oligo*-oxyethylene methacrylate) [PS-*b*-POEM] in the XPS with C_{60}^+ etching and NR studies). For the case of a homopolymer-blended BP electrolyte to be described herein, it is necessary to understand the salt distribution and correlate it to the homopolymer distribution because the lithium salt may interact preferentially with the BP or homopolymer.

In this work, we determined the salt and polymer distributions and used these distributions to understand the bulk conductivity trends in BP/homopolymer blended electrolytes doped with lithium trifluoromethanesulfonate (lithium triflate) salt. The spatial distributions of the lithium triflate salt were elucidated, as a function of homopolymer molecular weight and lithium salt concentration, using NR. As described previously, the natural scattering length density (SLD) contrast between the lithium salt and the two polymer blocks promoted the determination of the salt distribution.[39] The same samples were probed with X-ray reflectometry (XRR) to establish

the polymer interfacial profile of the electrolyte blends. Blends with $\alpha < 1$ had lower interfacial widths than their unblended counterparts and significantly lower interfacial widths than blends with $\alpha > 1$. Using a strong-segregation theory (SST) approach, the dependences of the effective Flory-Huggins interaction parameter, χ_{eff}, and the statistical segment length of the POEM+salt, b_{POEM}, on the lithium salt concentration were calculated as a function of α and [EO]:[Li] in the blended electrolytes. By employing the combined XRR and NR profiles, the salt concentration in the POEM homopolymer was calculated, and the blend with $\alpha > 1$ had a significantly higher lithium salt concentration within the homopolymer than its $\alpha < 1$ counterpart.

The abovementioned structural insights then were combined with results from bulk electrolyte studies. The thermal properties were evaluated using differential scanning calorimetry (DSC); electrolytes with $\alpha < 1$ had a lower $T_{g,POEM}$ than their unblended or $\alpha > 1$ counterparts. The lithium mobility also was examined by ^{7}Li solid-state nuclear magnetic resonance (NMR) spectroscopy, and the electrolytes with $\alpha < 1$ had the highest lithium mobility, followed by the unblended and $\alpha > 1$ examples. Thus, the lithium mobility was related to the mobility of the POEM, which is defined as the difference between the operating temperature, T, and $T_{g,POEM}$. A transition temperature that corresponds to the lithium mobility, termed $T_{Li\ mobility}$, was established for each blend, and $T_{Li\ mobility}$ was correlated directly to the $T_{g,POEM}$ of the blends. Interestingly, despite the enhanced lithium mobility in the $\alpha < 1$ blend, the ionic conductivity was highest in the $\alpha > 1$ blend. This enhancement was attributed to the lower χ_{eff} and the more centralized homopolymer distribution in the $\alpha > 1$ blend. Furthermore, the unblended and $\alpha < 1$ blend conductivities fell onto a single curve once differences in the $T_{g,POEM}$ and volume fraction of conducting block were considered, but the $\alpha > 1$ blend conductivities remained higher. Overall, this combined analysis

was able to elucidate an alternate method to enhance the conductivity independently from the polymer segmental chain motion.

MATERIALS AND METHODS

Materials:

All chemicals were stored in an argon-filled glove box after purification and before use. Styrene (99%, stabilized, Acros Organics) and *oligo*-oxyethylene methyl ether methacrylate (OEM, > 99%, stabilized, Sigma-Aldrich, average molar mass = 500 g mol^{-1}) were purified by passage through a basic alumina column. The styrene was dried further by distilling it from calcium hydride. OEM and styrene were degassed *via* three freeze-pump-thaw cycles. Copper bromide [Cu(I)Br, 98%, Acros Organics] was purified by stirring in acetic acid for 30 min, filtering, washing twice with cold ethanol, and drying with dynamic vacuum. Anhydrous methanol (99.8%, Sigma-Aldrich) was stirred with calcium hydride, degassed *via* three freeze-pump-thaw cycles, and distilled. Ethyl 2-bromoisobutyrate (EBiB, 98%, Sigma-Aldrich), *N,N,N',N'',N'''*-pentamethyldiethylenetriamine (PMDETA, 99%, Sigma-Aldrich), and anisole (> 99%, Fisher Scientific) were degassed *via* three freeze-pump-thaw cycles. Dry tetrahydrofuran (THF, > 99%, optima, Fisher-Scientific) was degassed by purging with argon and dried on solvent purification columns. Lithium triflate (99.995%, Sigma-Aldrich) was dried at 150 °C for 48 h.

Polymer Synthesis and Characterization:

PS-*b*-POEM was synthesized according to literature protocols.[40] POEM homopolymers were made by atom transfer radical polymerization (ATRP) with EBiB as initiator. In a typical POEM polymerization, in an argon-filled glove box, Cu(I)Br (0.1 mmol), PMDETA (0.1 mmol), and

anisole were mixed to ensure full complexation of copper and ligand. Separately, OEM (2 – 10 mmol), EBiB (0.1 mmol), and anisole were combined in a round-bottom flask. To initiate the reaction, the copper solution was added to the reaction vessel, and then the flask was sealed. The reaction conversion was monitored by ^{1}H NMR (Bruker AV600III) spectroscopy with $CDCl_3$ (0.03 v/v% TMS) as a solvent, and the reaction was stopped by cooling with liquid nitrogen and then opening the reaction to air. The reaction mixture was purified by passage through a neutral alumina column to remove the copper and precipitated into mixtures of petroleum ether/diethyl ether/2-propanol (1/1/0.1 by volume). Size-exclusion chromatography (Viscotek VE2001) with THF as the eluent (1.0 mL min^{-1}) and PS standards (1,780 – 205,000 g mol^{-1}) was used to determine the molecular weight of the PS block, along with the dispersity of the POEM homopolymers and PS-*b*-POEM. The volume fraction of POEM in the PS-*b*-POEMs and the molecular weights of the POEM homopolymers were determined by ^{1}H NMR spectroscopy in $CDCl_3$ (0.03 v/v% TMS). The different PS-*b*-POEMs and POEMs, and their molecular properties, are listed in Table 1. All polymers were dried at 120 °C for 48 h before storage in a 0 °C freezer in an argon-filled glovebox.

Table 1. Polymer characteristics of polymers used in this study. The volume fraction of POEM is notated as f_{POEM} and is calculated using the bulk densities of the constituent homopolymers.

Polymer	**M_n (g mol^{-1})**	**$M_{n,POEM}$ (g mol^{-1})**	**Dispersity ($Đ$)**	**f_{POEM}**
PS-*b*-POEM-17.8	43,100	17,800	1.19	0.38
PS-*b*-POEM-23.9	42,200	23,900	1.21	0.53
POEM-8	8,000	8,000	1.13	1
POEM-24.1	24,100	24,100	1.08	1

Blend fabrication was performed in an argon-filled glove box, unless otherwise noted. PS-*b*-POEM/POEM blends (Table 2) were formulated by dissolving the desired PS-*b*-POEM and POEM in dry THF and allowing the solution to stir for at least 3 h. All blends were prepared with 20 wt% homopolymer. The blends were sealed in a drying chamber and dried under dynamic vacuum for 12 h. The homopolymer concentration was verified by ^{1}H NMR spectroscopy.

Table 2. Blend combinations used in this study. φ_H is the homopolymer volume fraction in the blend, and α is the ratio of the molecular weight of the POEM homopolymer to the molecular weight of the POEM block in the BP. Blends with $\alpha > 1$ were expected to exhibit dry-brush-like behavior, and blends with $\alpha < 1$ were anticipated to show wet-brush-like behavior.

Polymer blend	**BP**	**Homopolymer**	φ_H	α
Unblended-17.8	PS-*b*-POEM-17.8	N/A	0	---
Wet brush-17.8	PS-*b*-POEM-17.8	POEM-8	0.2	0.45
Dry brush-17.8	PS-*b*-POEM-17.8	POEM-24.1	0.2	1.35
Unblended-23.9	PS-*b*-POEM-23.9	N/A	0	---
Wet brush-23.9	PS-*b*-POEM-23.9	POEM-8	0.2	0.33
Dry brush-23.9	PS-*b*-POEM-23.9	POEM-24.1	0.2	1.01

Polymer Film Preparation:

Solutions of Unblended-17.8, Wet brush-17.8, Dry brush-17.8, and lithium triflate solutions were prepared in an argon-filled glove box by dissolving each material in dry THF at approximately 5 wt% and stirring for at least 3 h. The polymer and salt stock solutions were mixed

gravimetrically and stirred for 3 h to achieve the desired [EO]:[Li], ranging from 24:1 and 8:1. 15 wt% methanol was added to the electrolyte solutions to enable formation of higher-quality thin films;[38-39] in these cases, the final polymer/salt/THF/methanol solutions were ~ 3.5 wt% polymer.

Silicon wafer substrates (<100> orientation, Wafer World, Inc.) were rinsed with toluene three times and cleaned in an ultraviolet-ozone oven (model 342, Jelight Co., Inc.). Films were flow coated[41] to cast the salt-doped BPs and BP blends on the cleaned silicon substrates. Films with shallow thickness gradients (70 mm long, 25.4 mm wide, between 90 and 150 nm thick) were cast, and commensurate regions corresponding to 2.5 or 3.5 times the domain spacing (L_0) were used for NR and XRR experiments. The films were dried under vacuum overnight at room temperature before being annealed under dynamic vacuum for 6 h at 135 °C (for Unblended-17.8 and Wet brush-17.8) or 120 °C (for Dry brush-17.8). Film thicknesses were measured with spectral reflectometry using a Filmetrics F20-UV interferometer.

NR:

NR experiments were conducted on the multi-angle grazing-incidence k-vector (MAGIK) instrument[42] at the National Institute of Standards and Technology (NIST) Center for Neutron Research. Neutrons with an incident wavelength of 5 Å were used, and for each sample, scans of Q_z from 0 to 0.0877 Å^{-1} were recorded with a step size of 0.0004 Å^{-1}. To minimize the warping of the silicon substrates, elastic clamps were used with an aluminum sample holder, and a borated aluminum mask was added between the neutron source and the films to minimize scattering from the sample holder, clamps, and silicon wafers. The reflectometry profiles were reduced using

NIST's reductus software and analyzed with repeating lamellae models in the refl1D software program.[43-44]

XRR:

XRR experiments were conducted on a Rigaku Ultima IV X-ray Diffractometer. A Cu Kα X-ray source (λ = 1.54 Å) was used, and a thin, parallel X-ray beam was scanned over incident angles (θ) and detection angles (2θ) of $0° < 2\theta < 3°$ with a step size of 0.004° and a scan rate of 0.5° min^{-1}. The beam size was set such that the critical edge of the thin film sample was captured. Rigaku Globalfit software was used to fit the XRR profile with repeating lamellae models.

Bulk Electrolyte Fabrication:

Lithium salt solutions of lithium triflate and dry THF were allowed to stir for at least 3 h. Electrolytes were created by dissolving the desired amount of BP (PS-*b*-POEM-23.9) or BP blend (Wet brush-23.9 and Dry brush-23.9) in dry THF, stirring for at least 3 h, and adding the requisite lithium salt solution gravimetrically. The BP and BP blend electrolyte solutions were mixed for at least 3 h before they were sealed in drying chambers and dried under dynamic vacuum for about 12 h. Once fully dry, the electrolytes were stored in an argon-filled glove box until testing. This sample preparation method was used for all small-angle X-ray scattering (SAXS), DSC, ^{7}Li solid-state NMR spectroscopy, and alternating current (AC) impedance spectroscopy specimens.

SAXS:

All salt-doped SAXS samples were prepared in an argon-filled glove box by sealing between two Kapton films in a homemade sample holder to avoid absorption of moisture. SAXS was

conducted on a Xenocs instrument with a sealed-tube X-ray source (Cu Kα, λ = 1.54 Å) operating at 2.0 kW with a 2-D detector and 2000 mm sample-to-detector distance. The path tubes were held under dynamic vacuum to reduce scattering from air, and sample temperatures were controlled using a Linkam HFSX350-CAP stage under dynamic vacuum. All SAXS samples were annealed at 150 °C for 2 h, cooled to 120 °C for 4 h, and cooled further to 30 °C for 4 h under dynamic vacuum, and SAXS profiles were acquired at each temperature. The data reported herein were taken at 120 °C. All two-dimensional scattering data were azimuthally integrated, resulting in plots of scattered intensity *vs.* scattering vector, q.

DSC:

DSC experiments were performed on a TA Instruments Discovery DSC with an RCS90 cooling accessory. Samples were loaded in an argon-filled glove box and hermetically sealed in aluminum pans. Three heating/cooling cycles between -80 °C and 150 °C at 5 °C min^{-1} were used with a nitrogen atmosphere. Baseline calibration was conducted with sapphire disks, and temperature and cell constant calibrations were determined using an indium standard. The reported T_g was determined from the midpoint of the inflection in the third heating trace. The second and third heating were compared to ensure reproducibility upon heating.

^{7}Li NMR Spectroscopy:

^{7}Li NMR data were collected using a 300 MHz DMX300 Bruker NMR spectrometer with a 4-mm probe using the solid echo (π/2-τ-π/2-τ-Acq) and single π/2 pulse sequences with ^{1}H decoupling. Solid echoes were used for T < 47 °C. For T > 47 °C, solid echoes and single pulse excitation sequences yielded indistinguishable spectra. Each sample (16 – 29 mg) was sealed in a

Kel-F rotor insert in a dry glove box, placed into a ZrO_2 rotor, and loaded into the NMR probe that was purged with dry air (-100 °C dew point) to ensure samples did not encounter moisture. Typical NMR experimental parameters were: 116.64 MHz Larmor frequency, 3.5 μs π /2 pulse, 20 μs τ delay, 80 kHz ^{1}H continuous wave (cw) decoupling, 1 μs or 5 μs dwell time, 16384 receiver gain, 4096 data points, 61440 zero filled points, and 100 Hz apodization. Temperature was controlled to within ± 1 °C and was calibrated using a lead nitrate ^{207}Pb NMR standard.[45] For the variable temperature experiments, each sample was cooled to the lowest temperature (-70 °C) first, equilibrated for 15 min, and then scanned. Samples were equilibrated at subsequently warmer temperatures for 15 min prior to scanning. Experiments were performed at temperatures ranging from -70 °C to 137 °C.

AC Impedance Spectroscopy:

Salt-doped BPs and BP blends were pressed under elevated temperatures (150 °C) into disks under vacuum in an argon-filled glove box and placed into a homemade test cell on a Linkam HFS91 CAP stage as described previously.[46] To perform the ionic conductivity measurements, the test cell was connected to a Princeton Applied Research PARSTAT 2273 frequency response analyzer, and all measurements were taken under vacuum. Samples were heated to 120 °C for 2 h to promote good contact with the aluminum electrodes and then cooled to 20 °C. The impedance measurements were taken upon heating between 20 °C and 150 °C at 10 °C increments, holding at each temperature for 10 min. At a given temperature, two measurements were acquired and averaged. The AC frequency range and voltage amplitude were 0.1-1 MHz and 10 mV, respectively. The touchdown point in the Nyquist plot was defined as the bulk resistance, *R*, and

the ionic conductivity, σ, was calculated as $\sigma = L/(RA)$, in which L is the sample thickness, and A is the area between the electrolyte and electrode.

RESULTS

To probe the enhancement in conductivity for the homopolymer-blended BP composite electrolytes, the structural, thermal, and electrochemical properties were examined. As a result of the large parameter space (α, φ_H, $M_{n,BP}$, $M_{n,H}$, etc.), finding an appropriate balance of the homopolymer distribution, salt distribution, and overall ion conducting properties is challenging. To this end, we investigated the salt and polymer distributions in parallel-lamellae-forming thin films by NR and XRR, respectively. Next, we proxied the polymer and lithium mobilities by DSC and ^{7}Li NMR spectroscopy, respectively, to probe the effect of homopolymer molecular weight (and thus α) on thermal properties and ion environment. Finally, we measured the conductivity of the blended electrolytes and compared the effect of the salt and polymer distributions to the ion mobility to elucidate the primary conduction mechanisms in these composite electrolytes.

The neutron and X-ray SLDs ($\rho_{neutron}$ and $\rho_{X\text{-}ray}$, respectively) for the component materials used in this study are listed in Table 3. The $\rho_{neutron,Li\ triflate}$ is higher than either of the component polymers, and $\rho_{neutron,POEM}$ is less than $\rho_{neutron,PS}$; thus, as salt is added, a contrast match condition can be found when $\rho_{neutron,POEM+Li\ triflate} = \rho_{neutron,PS}$, as described previously for salt-doped BP electrolyte systems.[39]

Table 3. Neutron and X-ray SLDs.[47]

Material	Neutron SLD ($\rho_{neutron}$) ($\times 10^6$ Å^{-2})	X-ray SLD ($\rho_{X\text{-}ray}$) ($\times 10^6$ Å^{-2})
PS	1.41	9.61

POEM	0.78	11.30
Li triflate	3.08	15.86

NR profiles of films of Unblended-17.8, Wet brush-17.8, and Dry brush-17.8 doped with [EO]:[Li] ratios of 12:1 were collected on the MAGIK reflectometer (colored data points, Figure 1). At least one Bragg peak was identifiable in all three profiles, though they were much more prominent in Wet brush-17.8 (where, a second order peak, marked with a black arrow, also appears) than in either of the other films. As the homopolymer content changed, the interfacial roughness was affected, which was particularly illustrated by the rapid decay of the Kiessig fringes in the Dry brush-17.8 profile because of increased mixing between blocks. Additional profiles of films with different salt doping ratios ([EO]:[Li] = 24:1, 8:1, and 18:1) are provided in Figures S1, S2, and S3, respectively.

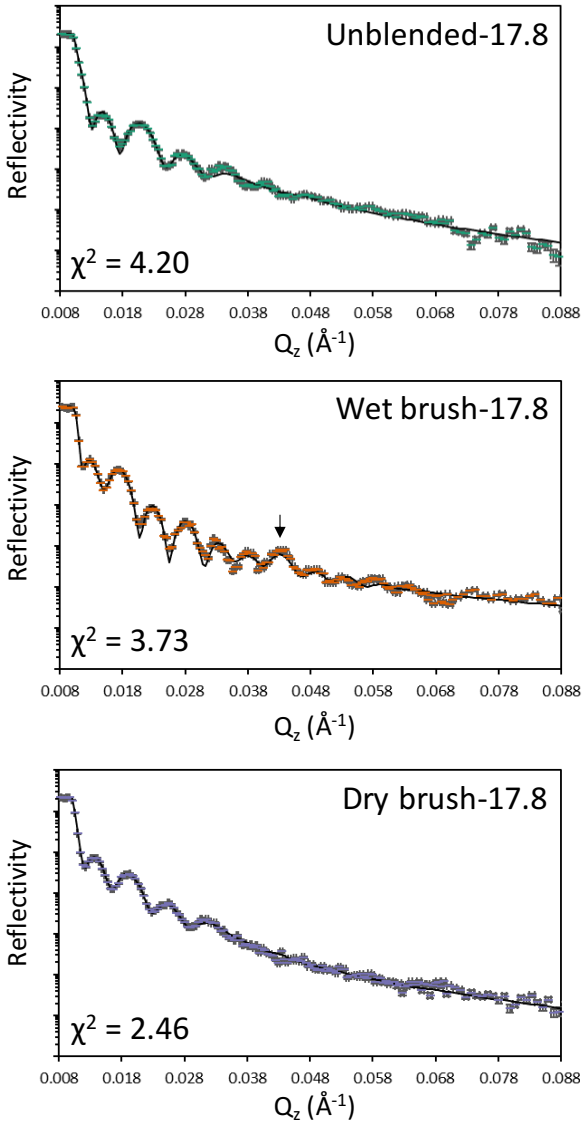

Figure 1. NR profiles (colored data points) and model fits (black lines) for Unblended-17.8 (green), Wet brush-17.8 (orange), and Dry brush-17.8 (purple) with [EO]:[Li] = 12:1. The black arrow indicates the second order peak in the Wet brush-17.8. Error bars and uncertainty represent one standard error. We note that the χ^2 reported in this manuscript is a measure of the statistical fitting of a model to the reflectometry data (using the normalized χ^2 test) and is not related to the Flory-Huggins parameter, χ_{eff}.

NR profiles were fit to repeating multilayer lamellae models, the outputs of which are shown in Figure 2; a representative fit at [EO]:[Li] = 12:1 is presented for Unblended-17.8, Wet brush-17.8, and Dry-brush 17.8. Multilayer models for the other salt concentrations are included in Figures S1-S3. The $\rho_{neutron}$ profiles are plotted as a function of the depth through the film in Figures 2 and S1-S3. To reduce the number of fitting parameters, the following constraints were applied. The value of $\rho_{neutron,PS}$ was held close (within 0.05×10^6 Å^{-2}) to the value for the neat PS, as it has been established that lithium salts are not found in the PS domains.[35, 38-39] Additionally, for each respective sample, all interior PS and interior POEM+salt domains had similar model parameters (layer thicknesses, SLDs, and interfacial widths). This approach allowed us to determine average properties of the interior region, separate from the interfacial POEM and surface PS layers. This route was chosen (as opposed to a multilayer model with more degrees of freedom) to identify more physically relevant solutions, as opposed to those that just minimized χ^2. In all cases, there was a reduced SLD at the polymer/substrate interface, likely due to small amounts of solvent trapped at the substrate.

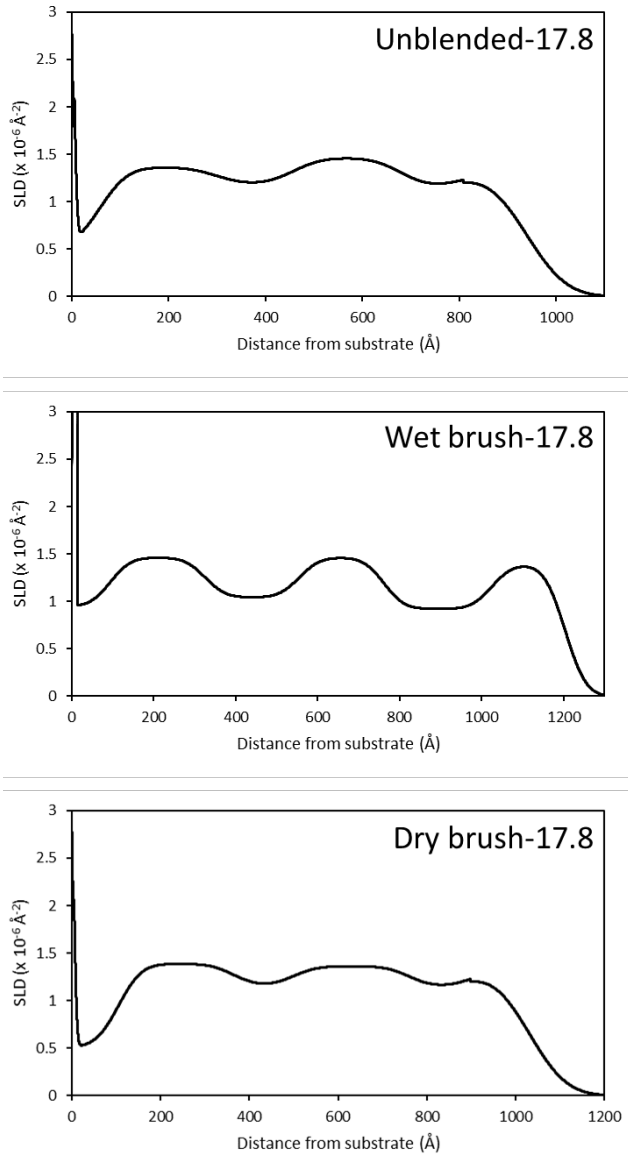

Figure 2. SLD profiles for Unblended-17.8, Wet brush-17.8, and Dry brush-17.8, at [EO]:[Li] = 12:1, as a function of distance from the substrate surface.

The same films (Unblended-17.8, Wet brush-17.8, and Dry brush-17.8) were probed using XRR to quantitively determine the domain spacing (d) and interfacial roughness (f_{int}) between the PS and POEM domains; see Figure 3. As expected, the d of the blended BP electrolytes generally was higher than that of the unblended samples (Figure 3a) across all salt concentrations.

Furthermore, for the blended samples, the wet brush had a higher d than the dry brush, consistent with results from other systems with low φ_H.[30, 48] For all samples, d increased linearly with increasing r = [Li]/[EO], and all blend types had similar linear scaling. The f_{int} (Figure 3b) was defined as two times the average interfacial width (t_{int}) between PS and POEM domains, normalized by the domain spacing, which provided a measure of the relative amount of the lamellar period contained within the interfacial region between domains. f_{int} is defined in Equation 1:

$$f_{int} = \frac{2t_{int}}{d} = \frac{2(2\pi)^{\frac{1}{2}}\delta}{d} \quad (1)$$

in which δ is the roughness parameter from the Rigaku GlobalFit software.[39, 49-50] f_{int} generally decreased as r increased, and Dry brush-17.8 had the highest interfacial widths across all salt concentrations. Additional XRR profiles and fits for all samples are shown in Figure S4.

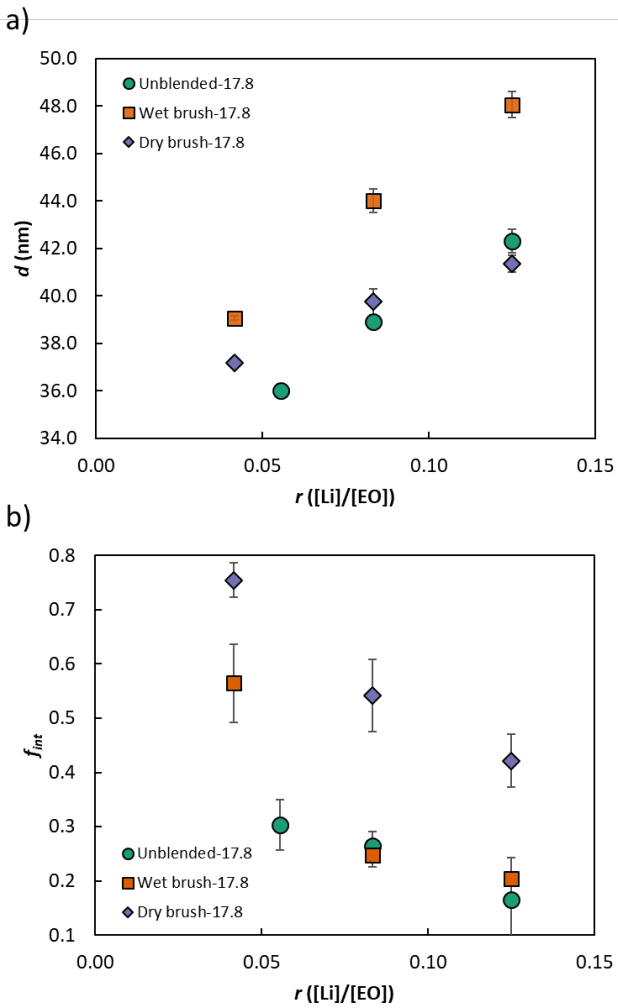

Figure 3. (a) Domain spacing *d*, and (b) volume fraction of interface, f_{int}, as a function of Li triflate salt concentration, *r*, for Unblended-17.8 (green circles), Wet brush-17.8 (orange squares), and Dry brush-17.8 (purple diamonds) specimens. *d* increased and f_{int} decreased as *r* increased for all blend conditions. The error bars in (a) represent the standard deviation in layer thickness from the XRR fits, and the error bars in (b) are propagated uncertainties of the roughness parameter from XRR fits. If error bars are not visible, the error is smaller than the size of the data point.

With an enhanced understanding of the salt and polymer distributions of the blended electrolytes, bulk characterization was performed using a different (relative to the reflectometry studies) parent

block polymer to generate Unblended-23.9, Wet brush-23.9, and Dry-brush-23.9 samples doped with Li triflate at [EO]:[Li] = 16:1. Due to the higher volume fraction of POEM in PS-*b*-POEM-23.9, upon doping with Li triflate, a hexagonally-packed cylindrical morphology was formed in all blended samples, as suggested by the peaks indexed to 1, √3, and 2 in the SAXS profiles (Figure S5). It must be noted that the ion transport behavior of BP electrolytes is affected by the nanostructured morphology; however, it has been established by Matsen that the homopolymer distribution is similar between hexagonally-packed cylinders and lamellae.[29] Thus, it is assumed that these studies are relevant to both morphologies, and the insights gleaned from the NR and XRR studies can be used to understand the bulk characterizations herein.

First, as ionic conductivity in polymer electrolytes is related to the segmental chain motion of the polymer, we used DSC to examine the thermal transitions in the blends. The DSC traces for the three samples are shown in Figure 4, and the $T_{g,POEM,}$, $T_{g,PS}$, and change in heat capacity of the $T_{g,POEM}$ ($\Delta c_{P,POEM}$) are given in Table 4. Two transitions were clearly visible in each trace, which corresponded to $T_{g,POEM}$ (-47 to -43 °C) and $T_{g,PS}$ (93 to 95 °C), though $T_{g,POEM}$ was a more prominent transition, due to the higher mass fraction of POEM. For all samples, $T_{g,PS}$ was close to the predicted homopolymer $T_{g,PS}$ at this molecular weight on the basis of the empirical equation suggested by Flory and Fox,[51] indicating that there was little mixing between the blocks. $T_{g,POEM}$ was lowest in Wet brush-23.9 and highest in Dry brush-23.9, with Unblended-23.9 falling in between. Though these differences are small, they are relative to the distinct instrument resolution, and small changes in T_g can correspond to sizable differences in the ionic conductivity (~20% increase in conductivity at 40 °C by decreasing $T_{g,POEM}$ from -43.5 to -47.0 °C).[52] $\Delta c_{P,POEM}$ was calculated by measuring the difference in height of the extrapolated baselines above and below $T_{g,POEM}$, and Wet brush-23.9 has the highest $\Delta c_{P,POEM}$ whereas Dry brush-23.9 has the lowest value.

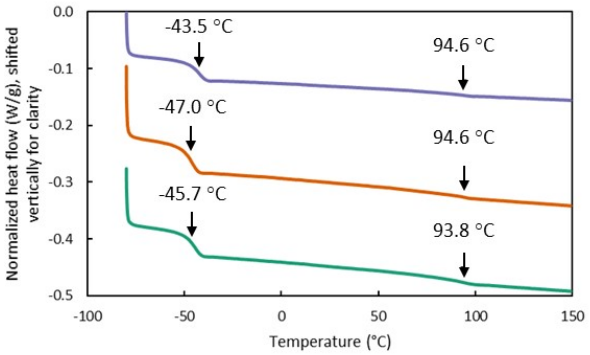

Figure 4. DSC trace on third heating (5 °C min^{-1}, N_2) for Unblended-23.9 (green), Wet brush-23.9 (orange), and Dry brush-23.9 (purple) samples, normalized by the total blended BP electrolyte mass. The curves are shifted vertically for clarity.

Table 4. DSC data for the BP blends.

Polymer blend	$T_{g,POEM}$ (°C)	$T_{g,PS}$ (°C)	$\Delta c_{P,POEM}$
Unblended-23.9	-45.7	93.8	0.43
Wet brush-23.9	-47.0	94.6	0.50
Dry brush-23.9	-43.5	94.6	0.36

Although the polymer thermal transitions often are considered as a reasonable proxy for the lithium mobility, it was possible to probe the lithium mobility directly using solid-state ^{7}Li linewidths. At temperatures for which the lithium still behaved as if in a glass (less than -30 °C), Li-O 'bonds' were in the rigid limit, and two resonances were identified: a narrow Lorentzian resonance and a broad Gaussian resonance, which were due to central (- 1/2 to 1/2) and satellite (-3/2 to -1/2, and 1/2 to 3/2) transitions, respectively, in the quadrupolar nuclei. As the temperature increased above the $T_{g,POEM}$, the Li-O 'bonds' broke or reoriented on < 100 μs (= $\pi/\Delta\nu$) timescales

(ν is the FWHM of the Gaussian resonance) such that both the intensity and breadth of the Gaussian curve decreased at the expense of the Lorentzian resonance, which also narrowed further upon heating. Generally, in this fast fluctuation limit, narrower peaks indicate more mobile lithium species.[53-54] An example of curves at two different temperatures is provided in Figure S6. The full width at half maximum of the fitted Lorentzian resonances of the Unblended-23.9, Wet brush-23.9, and Dry brush-23.9 samples are shown in Figure 5. The lithium mobilities in all blend conditions were high (approaching the 100 Hz of apodization applied to the time domain signal), but the Dry brush-23.9 lithium mobility was significantly lower than the other two mobilities.

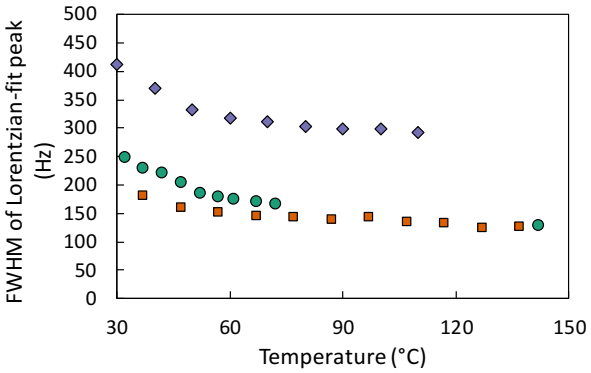

Figure 5. Full width, half maxima of Lorentzian fit peaks from ^{7}Li NMR spectra as a function of temperature for Unblended-23.9 (green circles), Wet brush-23.9 (orange squares), and Dry brush-23.9 (purple diamonds).

To determine the impact of homopolymer-blending on the ionic conductivity, AC impedance experiments were conducted on the Unblended-23.9, Wet brush-23.9, and Dry brush-23.9 samples doped with Li triflate at the salt-doping ratio of [EO]:[Li] = 16:1. The conductivity profiles as a function of inverse temperature are shown in Figure 6a. At all temperatures, Dry brush-23.9 exhibited the highest ionic conductivity, followed by Wet brush-23.9 and then Unblended-23.9.

The conductivities were fit to the nonlinear Vogel-Fulcher-Tammann (VFT) equation (Equation 2):

$$\sigma = \sigma_o e^{\frac{-B}{T-T_o}} \quad (2)$$

in which σ_o is the pre-exponential factor proportional to the number of charge carriers, B is an effective activation energy, T is the operating temperature, and T_o is a reference temperature, chosen as $T_o = T_{g,POEM} - 50$ K. By plotting conductivity as a function of T/T_g, and normalizing by the volume fraction of POEM (Figure 6b), additional factors that influence conductivity can be emphasized.[17, 52, 55] Fitting parameters are provided in Table S2.

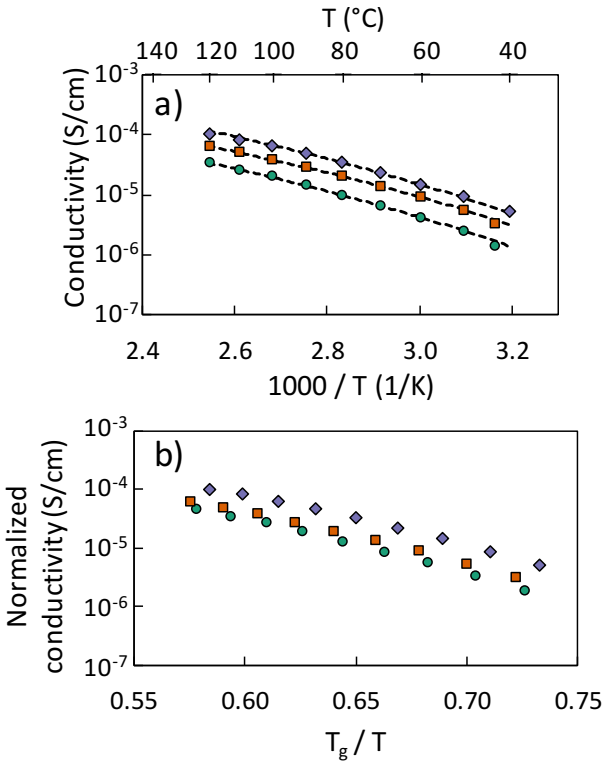

Figure 6. a) Ionic conductivity as a function of 1000/T, and b) ionic conductivity normalized by the volume fraction of total POEM as a function of T_g/T, for Unblended-23.9 (green circles), Wet brush-23.9 (orange squares), and Dry brush-23.9 (purple diamonds) samples.

DISCUSSION

These combined results highlight the competition between brush regime and mobility in blended BP electrolytes. In terms of structure, NR and XRR were used to infer the salt and polymer distributions in the electrolyte. From NR, the results were consistent with the hypothesis that the salt distribution followed the total POEM polymer distribution in all blend conditions. The two homopolymer profiles as a function of the normalized position in the POEM domain (x/l_{POEM}) are shown in Figure 7, and calculations are detailed in the Supporting Information. The Dry brush-17.8 homopolymer distribution was calculated using the analytical expressions developed by Shull and Winey with the polymer characteristics calculated from the XRR data herein.[27] The Wet brush-17.8 homopolymer distribution, as a result of the more complex nature of wet brush distributions, was fit to the homopolymer profile of the closest values of α and $\Phi_{homopolymer}$ from the same study (α = 0.52 *vs*. 0.45, $\Phi_{homopolymer}$ = 0.31 *vs*. 0.38).[27] Using these homopolymer distributions (Figure 7a), the salt doping ratio in the homopolymer POEM was determined algebraically. From these results (Figure 7b), it is clear that the homopolymer in the dry brush regime has a significantly higher salt concentration, reaching a minimum value of [EO]:[Li] in the center of the domain at [EO]:[Li] = 13:1 *vs*. 20:1 in Wet brush-17.8. Therefore, because the POEM homopolymer was more centrally localized in Dry brush-17.8, the salt concentration is enhanced within the homopolymer regime.

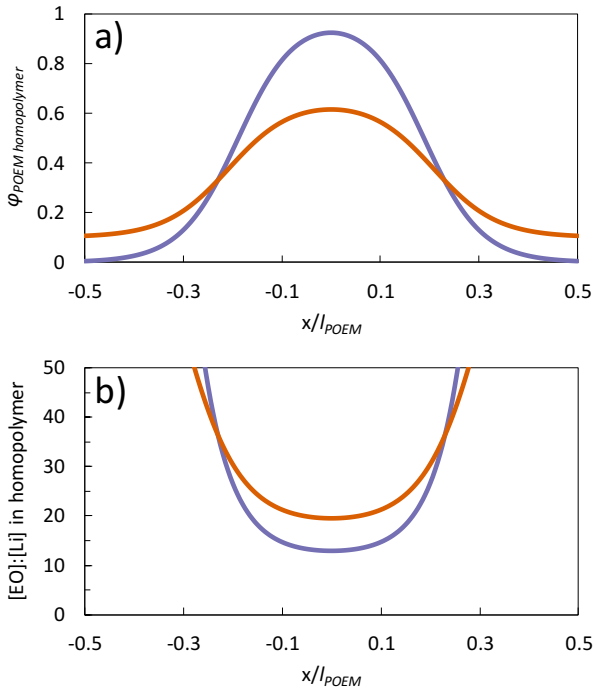

Figure 7. a) Fraction of homopolymer POEM within the POEM domain, and b) [EO]:[Li] in the homopolymer POEM as a function of x/l_{POEM} (position in POEM domain) for Dry brush-17.8 (purple) and Wet brush-17.8 (orange) doped at [EO]:[Li] = 12:1.

The XRR results were analyzed using SST to examine how the lithium salt interacted with the BP blends. For the Unblended-17.8 samples, the parameters determined from XRR (d, f_{int}, and the densities of each of the components) were combined with properties of the BP (N, φ_{POEM}, and the statistical segment length of PS) to calculate χ_{eff} and b_{POEM}.[39] For the homopolymer-blended BPs, the effective N_{POEM} was determined by ^{1}H NMR spectroscopy. The calculated χ_{eff} and b_{POEM} are plotted in Figure 8. The statistical segment length of PS was assumed to be constant at b_{PS} = 0.68 nm, and a reference volume ν_0 = 0.668 nm^3 (the volume of one POEM monomer) was used for all samples.[52, 56] As the salt concentration increased, b_{POEM} increased for Unblended-17.8 and Wet brush-17.8; for Dry brush-17.8, there was a slight decrease in b_{POEM} at high salt concentrations,

which was indicative of the brush architecture, as the homopolymer, which was segregated to the center of the POEM domain especially in the dry brush sample, had a higher ion concentration. Similarly, χ_{eff} increased with higher salt concentrations for all samples, and Dry brush-17.8 had the lowest χ_{eff}, while Unblended-17.8 had the highest χ_{eff}. We hypothesize that the different dependencies of χ_{eff} as a function of r was caused by the dry brush, homopolymer-rich regime, which led to a lower effective salt concentration in the BP-rich region of the self-assembled nanostructure. These differences in homopolymer blending therefore influenced the structure of the resulting electrolytes.

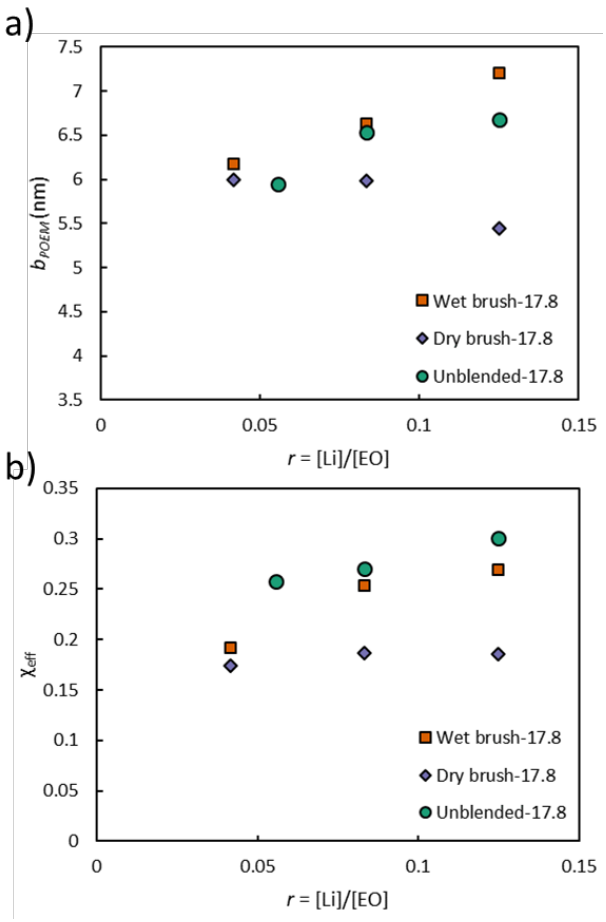

Figure 8. a) POEM statistical segment length (b_{POEM}) and b) effective Flory-Huggins interaction parameter (χ_{eff}) as a function of r for Unblended-17.8 (green circles), Wet brush-17.8 (orange squares), and Dry brush-17.8 (purple diamonds) specimens.

The interfacial width trends determined by XRR were supported by the thermal behavior established through DSC studies. $\Delta c_{P,POEM}$ (Table 4) was highest in Wet brush-23.9, followed by Unblended-23.9, and then Dry brush-23.9. Using the scaling from Morese-Seguela *et al.*, it follows that the thickness of interfacial region can be estimated from Equation 3,

$$t_{POEM} = \frac{L_{POEM}}{2}\left(1 - \frac{\Delta c_{P,POEM}}{\Delta c_{P,pure\ POEM}}\right) \quad (3)$$

in which L_{POEM} is a characteristic length scale of the POEM layer, and $\Delta c_{P,pure\ POEM}$ is the heat capacity change at T_g for homopolymer POEM.[57] Because of local salt concentration fluctuations, determination of $\Delta c_{P,pure\ POEM}$ at the comparative salt concentration of [EO]:[Li] = 16:1 is difficult, but the general trend that the highest $\Delta c_{P,POEM}$ (such as in Wet brush-23.9) corresponded to the lowest interfacial widths is nonetheless informative and matches the trends elucidated in this work.

The combination of DSC and ^{7}Li solid-state NMR spectroscopy enhanced understanding of the interplay between polymer and lithium mobilities. $T_{g,POEM}$ was inversely correlated to the lithium mobility as shown in Figure 9 such that the blended sample with the lowest $T_{g,POEM}$ had the highest lithium mobility. These differences in lithium mobility that occur more than 100 °C above the polymer electrolyte's T_g highlight the need to continue to develop ion-conducting polymers with depressed T_gs as a way to improve the lithium mobility.

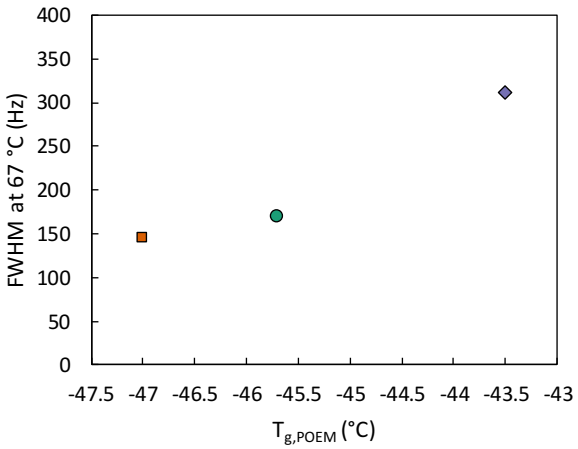

Figure 9. Full-width, half-maximum of the Lorentzian fit at 67 °C *vs.* $T_{g,POEM}$ for the Unblended-23.9 (green circles), Wet brush-23.9 (orange squares), and Dry brush-23.9 (purple diamonds) samples.

The temperature dependence of the motional narrowing of the broad ^{7}Li resonance also revealed a new characteristic temperature relevant to the mobility of lithium through polymer electrolytes. The broad peak, which represents the population of ^{7}Li spins involved in rigid Li-O 'bonds', became narrow upon heating due to the breaking and fast re-orientations of these Li-O bonds, causing scrambling of the three principal components of the Li quadrupolar tensor. When these events occurred on a time scale (t) faster than the inverse of the ^{7}Li linewidth ($t << \pi/30000$ Hz $\approx$ 10 μs), these three components became dynamically averaged. To further investigate this dynamic process, we aimed to quantify the temperature range over which this transition occurs, and the transition temperature, termed $T_{Li\ mobility}$, was defined as the mid-point of the transition. Representative curves for Unblended-23.9, Wet brush-23.9, and Dry brush-23.9 are shown in Figure 10. Curves were empirically fit to match the sigmoidal shape of the curves by minimizing the weighted sum of squares error *via* Equation 4,

$$I = K * \tan^{-1}\left(\frac{T-T_o}{T_f-T_o}\right) \quad (4)$$

in which I is the full width at half maximum of the Gaussian peak, K is a fitting parameter to capture the magnitude of the quadrupolar tensor in units of Hz, T is the temperature of interest, T_o is the onset of the transition, and T_f is the end of the transition. $T_{Li\ mobility}$ was defined as the midpoint of T_o and T_f. From these fits, $T_{Li\ mobility}$ was -6.0 °C for Unblended-23.9, -8.4 °C for Wet brush-23.9, and -4.9 °C for Dry brush-23.9. It is notable that this transition occurred at 39.0 ± 0.6 °C above $T_{g,POEM}$ in all the blends ($T_{g,POEM}$ = -45.7 °C for Unblended-23.9, -47.0 °C for Wet brush-23.9, and -43.5 °C for Dry brush-23.9), which was consistent with the idea that the motion of the ethylene oxide containing segments were responsible for breaking the Li-O bonds and, furthermore, indicates that $T_{Li\ mobility}$ may be a more representative measure of the temperature at which most of the lithium ions in the electrolyte are mobile. It is expected that the difference

between $T_{g,polymer}$ and $T_{Li\ mobility}$ is a polymer- and lithium-salt-dependent property, and examining this difference in a variety of lithium salts and polymers will be fruitful in the development of electrolyte systems.

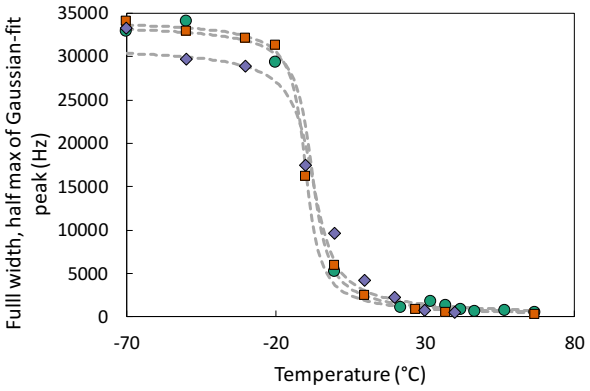

Figure 10. Full width, half maximum of the Gaussian fit from ^{7}Li linewidth NMR spectroscopy as a function of temperature for Unblended-23.9 (green circles), Wet brush-23.9 (orange squares), and Dry brush-23.9 (purple diamonds). Fits to Equation 4 are shown with grey dashed lines.

The discrepancy between the enhanced lithium mobility in Wet brush-23.9 and the enhanced ionic conductivity in Dry brush-23.9 provokes questions about the relative importance of mobility *vs*. brush regime. As noted in Figure 6b, by normalizing by the $T_{g,\ POEM}$ and φ_{POEM}, Unblended-23.9 and Wet brush-23.9 collapse onto a single curve, likely indicating that their conduction mechanism is similar. It is straightforward to rationalize these similarities on the basis of the structural characterizations by NR and XRR, as the wet brush acts like a plasticized version of the unblended BP electrolyte. The VFT fits to the conductivity (Table S2), shown with the grey lines in Figure 6a, indicated that there was little difference in the *B* parameter, which relates to the effective activation energy. Moreover, the *B* parameters were all similar to tapered PS-*b*-POEM doped with Li triflate electrolytes at [EO]:[Li] = 15:1,[52] suggesting a similar conduction

mechanism in all of these samples. The effective ion concentration, which is related to the pre-exponential factor, σ_o, was twice as large for Dry brush-23.9 ($\sigma_o = 2.2 \times 10^{-2}$ S cm^{-1}) than Wet brush-23.9 ($\sigma_o = 1.1 \times 10^{-2}$ S cm^{-1}), which correlated to the homopolymer salt concentration being approximately twice as high in Dry brush-23.9 and was close to the calculated result in Figure 7b. This difference implies that the region consisting of majority homopolymer is better able to conduct ions. Thus, though lithium mobility was higher in Wet brush-23.9 than Dry brush-23.9, the higher salt concentration in the homopolymer-rich regime in Dry brush-23.9 had a stronger effect on the ionic conductivity.

CONCLUSIONS

We report a strategy to introduce homopolymer-rich conducting pathways in BP composite electrolytes to improve ionic conductivity. The lithium salt and polymer distributions were probed by NR and XRR. NR was harnessed to determine the lithium salt profiles, and the results were consistent with fits in which the lithium salt followed the POEM profile. Polymer interfacial profiles, including the domain spacings and interfacial widths, were determined using XRR; Wet brush-17.8 had the lowest interfacial widths, and Dry brush-17.8 had the highest interfacial widths across all salt concentrations. The homopolymer profiles were used to calculate the effective salt concentration in the POEM homopolymers, and, despite having the same overall salt concentration, the Dry brush-17.8 had a significantly higher maximum salt concentration in the POEM homopolymer. By combining the XRR results with SST, the dry brush-blended system had the lowest effective Flory-Huggins parameter across all salt concentrations, indicating higher compatibility between blocks. In bulk electrolyte materials, the wet brush-blended electrolytes demonstrated a depressed $T_{g,POEM}$ and the highest lithium mobility, as determined by DSC and ^{7}Li

NMR linewidth measurements. From the ^{7}Li NMR, a new relevant temperature for lithium conduction, $T_{Li\ mobility}$, was defined as the mid-point temperature between lithium-oxide bonds being completely rigid in a glassy polymer electrolyte matrix and being completely broken leaving lithium free to move amongst the polymer matrix on time scales faster than 10 μs. This transition temperature was found to follow the same trend as $T_{g,POEM}$, and for all samples probed, $T_{Li\ mobility}$ was 39 °C above $T_{g,POEM}$. The ionic conductivity was probed *via* AC impedance spectroscopy, and despite its suppressed lithium mobility, the dry brush-blended electrolyte demonstrated the highest ionic conductivity. This enhancement was attributed to the higher salt concentration in the homopolymer-rich regime, which led to an overall increase in the fraction of mobile ions. Taken together, these insights demonstrate the complex nature of maximizing the ionic conductivity in a BP electrolyte material, as both structure and inherent mobility are key in the performance of these materials.

ASSOCIATED CONTENT

Supporting Information. Blend compositions; NR multilayer model fits for Unblended-17.8, Wet brush-17.8, and Dry brush-17.8 samples at [Li]:[EO] = 24:1, 8:1; XRR profiles and fits; SAXS profiles; representative spectra of ^{7}Li solid-state NMR spectroscopy of Dry brush-23.9 at -70 °C and 57 °C; description of the homopolymer distribution calculations; VFT fits of the ionic conductivity

AUTHOR INFORMATION

Corresponding Author

*Email: thepps@udel.edu

Author Contributions

The manuscript was written through contributions of all authors. All authors have given approval to the final version of the manuscript.

Funding Sources

Department of Energy (DOE BES (DE-SC0014458))

National Institute of Standards and Technology (NIST-70NANB12H239)

National Institutes of Health (NIGMS (5 P30 GM110758-02))

National Science Foundation (NSF DMR-1610134)

Thomas & Kipp Gutshall Professorship

ACKNOWLEDGMENT

M.A.M., P.M.K., and T.H.E. thank a Department of Energy grant (DOE BES (DE-SC0014458)) for polymer synthesis, characterization, and film casting. The NR experiments were conducted under cooperative agreement 70NANB12H239 from NIST, U.S. Department of Commerce. S.H.S. thanks National Science Foundation (NSF DMR-1610134) for supporting the XRR characterization efforts. The solution-state NMR operations at UD were partially supported by the

Delaware COBRE program, with a grant from the National Institute of General Medical Sciences – NIGMS (5 P30 GM110758-02) from the National Institutes of Health (NIH). T.H.E. also thanks the Thomas & Kipp Gutshall Professorship for financial support. The statements, findings, conclusions, and recommendations are those of the authors and do not necessarily reflect the views of NIST, the U.S. Department of Commerce, or the NSF. Certain commercial equipment, instruments, materials, suppliers, or software are identified in this paper to facilitate understanding and interpretation of data. Such identifications do not imply recommendation or endorsement by NIST, NSF, DOE, or NIH, nor do they imply that the materials or equipment identified are necessarily the best available for the purpose.

REFERENCES

1. Armand, M.; Tarascon, J. M., Building Better Batteries. *Nature* **2008,** *451*, 652-657.
2. Goodenough, J. B.; Park, K. S., The Li-Ion Rechargeable Battery: A Perspective. *Journal of the American Chemical Society* **2013,** *135* (4), 1167-1176.
3. Arora, P.; Zhang, Z. M., Battery separators. *Chem. Rev.* **2004,** *104* (10), 4419-4462.
4. Brissot, C.; Rosso, M.; Chazalviel, J. N.; Baudry, P.; Lascaud, S., In situ study of dendritic growth in lithium/PEO-salt/lithium cells. *Electrochimica Acta* **1998,** *43* (10-11), 1569-1574.
5. Meyer, W. H., Polymer electrolytes for lithium-ion batteries. *Advanced Materials* **1998,** *10* (6), 439-448.
6. Armand, M. B., Polymer Electrolytes. *Annual Review of Materials Science* **1986,** *16*, 245-261.
7. Hallinan, D. T.; Balsara, N. P., Polymer Electrolytes. *Ann. Rev. Mater. Res.* **2013,** *43*, 503-525.
8. Ruzette, A. V. G.; Soo, P. P.; Sadoway, D. R.; Mayes, A. M., Melt-formable block copolymer electrolytes for lithium rechargeable batteries. *Journal of the Electrochemical Society* **2001,** *148* (6), A537-A543.
9. Jangu, C.; Savage, A. M.; Zhang, Z. Y.; Schultz, A. R.; Madsen, L. A.; Beyer, F. L.; Long, T. E., Sulfonimide-Containing Triblock Copolymers for Improved Conductivity and Mechanical Performance. *Macromolecules* **2015,** *48* (13), 4520-4528.
10. Kim, O.; Kim, S. Y.; Lee, J.; Park, M. J., Building Less Tortuous Ion-Conduction Pathways Using Block Copolymer Electrolytes with a Well-Defined Cubic Symmetry. *Chem. Mat.* **2016,** *28* (1), 318-325.
11. Qin, J.; de Pablo, J. J., Ordering Transition in Salt-Doped Diblock Copolymers. *Macromolecules* **2016,** *49* (9), 3630-3638.
12. Chintapalli, M.; Le, T. N. P.; Venkatesan, N. R.; Mackay, N. G.; Rojas, A. A.; Thelen, J. L.; Chen, X. C.; Devaux, D.; Balsara, N. P., Structure and Ionic Conductivity of Polystyrene-block-poly(ethylene oxide) Electrolytes in the High Salt Concentration Limit. *Macromolecules* **2016,** *49* (5), 1770-1780.
13. Sethuraman, V.; Mogurampelly, S.; Ganesan, V., Multiscale Simulations of Lamellar PS–PEO Block Copolymers Doped with $LiPF_6$ Ions. *Macromolecules* **2017,** *50* (11), 4542-4554.
14. Maslyn, J. A.; Loo, W. S.; McEntush, K. D.; Oh, H. J.; Harry, K. J.; Parkinson, D. Y.; Balsara, N. P., Growth of Lithium Dendrites and Globules through a Solid Block Copolymer Electrolyte as a Function of Current Density. *The Journal of Physical Chemistry C* **2018,** *122* (47), 26797-26804.
15. Elabd, Y. A.; Hickner, M. A., Block Copolymers for Fuel Cells. *Macromolecules* **2011,** *44* (1), 1-11.
16. Morris, M. A.; Gartner, T. E., III; Epps, T. H., III, Tuning Block Polymer Structure, Properties, and Processability for the Design of Efficient Nanostructured Materials Systems. *Macromolecular Chemistry and Physics* **2017,** *218* (5), 1600513.
17. Ketkar, P. M.; Shen, K.-H.; Hall, L. M.; Epps, T. H., III, Charging toward improved lithium-ion polymer electrolytes: exploiting synergistic experimental and computational approaches to facilitate materials design. *Molecular Systems Design & Engineering* **2019,** *4* (2), 223-238.

18. Ganesan, V.; Pyramitsyn, V.; Bertoni, C.; Shah, M., Mechanisms Underlying Ion Transport in Lamellar Block Copolymer Membranes. *ACS Macro Letters* **2012,** *1* (4), 513-518.
19. Dong, B. X.; Bennington, P.; Kambe, Y.; Sharon, D.; Dolejsi, M.; Strzalka, J.; Burnett, V. F.; Nealey, P. F.; Patel, S. N., Nanothin film conductivity measurements reveal interfacial influence on ion transport in polymer electrolytes. *Molecular Systems Design & Engineering* **2019,** *4* (3), 597-608.
20. Harry, K. J.; Hallinan, D. T.; Parkinson, D. Y.; MacDowell, A. A.; Balsara, N. P., Detection of Subsurface Structures Underneath Dendrites Formed on Cycled Lithium Metal Electrodes. *Nature Materials* **2014,** *13* (1), 69-73.
21. Harry, K. J.; Parkinson, D. Y.; Balsara, N. P., Failure Analysis of Batteries Using Synchrotron-based Hard X-ray Microtomography. *J. Vis. Exp.* **2015,** (102), e53021.
22. Morris, M. A.; An, H.; Lutkenhaus, J. L.; Epps, T. H., III, Harnessing the Power of Plastics: Nanostructured Polymer Systems in Lithium-Ion Batteries. *ACS Energy Lett.* **2017,** *2* (8), 1919-1936.
23. Young, W. S.; Kuan, W. F.; Epps, T. H., III, Block Copolymer Electrolytes for Rechargeable Lithium Batteries. *Journal of Polymer Science Part B-Polymer Physics* **2014,** *52* (1), 1-16.
24. Weber, R. L.; Ye, Y. S.; Schmitt, A. L.; Banik, S. M.; Elabd, Y. A.; Mahanthappa, M. K., Effect of Nanoscale Morphology on the Conductivity of Polymerized Ionic Liquid Block Copolymers. *Macromolecules* **2011,** *44* (14), 5727-5735.
25. Kambe, Y.; Arges, C. G.; Patel, S.; Stoykovish, M. P.; Nealey, P. F., Ion Conduction in Microphase-Separated Block Copolymer Electrolytes. *The Electrochemical Society Interface* **2017,** *26* (1), 61-67.
26. Winey, K. I.; Thomas, E. L.; Fetters, L. J., Swelling of lamellar diblock copolymer by homopolymer: influences of homopolymer concentration and molecular weight. *Macromolecules* **1991,** *24* (23), 6182-6188.
27. Shull, K. R.; Winey, K. I., Homopolymer distributions in lamellar copolymer/homopolymer blends. *Macromolecules* **1992,** *25* (10), 2637-2644.
28. Winey, K. I.; Thomas, E. L.; Fetters, L. J., Isothermal Morphology Diagrams for Binary Blends of Diblock Copolymer and Homopolymer. *Macromolecules* **1992,** *25* (10), 2645-2650.
29. Matsen, M. W., Phase Behavior of Block Copolymer/Homopolymer Blends. *Macromolecules* **1995,** *28* (17), 5765-5773.
30. Mayes, A. M.; Russell, T. P.; Satija, S. K.; Majkrzak, C. F., Homopolymer Distributions in Ordered Block Copolymers. *Macromolecules* **1992,** *25* (24), 6523-6531.
31. Koizumi, S.; Hasegawa, H.; Hashimoto, T., Spatial Distribution of Homopolymers in Block Copolymer Microdomains as Observed by a Combined SANS and SAXS Method. *Macromolecules* **1994,** *27* (26), 7893-7906.
32. Doerk, G. S.; Yager, K. G., Rapid Ordering in "Wet Brush" Block Copolymer/Homopolymer Ternary Blends. *ACS Nano* **2017,** *11* (12), 12326-12336.
33. Irwin, M. T.; Hickey, R. J.; Xie, S.; Bates, F. S.; Lodge, T. P., Lithium Salt-Induced Microstructure and Ordering in Diblock Copolymer/Homopolymer Blends. *Macromolecules* **2016,** *49* (13), 4839-4849.
34. Irwin, M. T.; Hickey, R. J.; Xie, S.; So, S.; Bates, F. S.; Lodge, T. P., Structure–Conductivity Relationships in Ordered and Disordered Salt-Doped Diblock Copolymer/Homopolymer Blends. *Macromolecules* **2016,** *49* (18), 6928-6939.

35. Gomez, E. D.; Panday, A.; Feng, E. H.; Chen, V.; Stone, G. M.; Minor, A. M.; Kisielowski, C.; Downing, K. H.; Borodin, O.; Smith, G. D.; Balsara, N. P., Effect of Ion Distribution on Conductivity of Block Copolymer Electrolytes. *Nano Lett.* **2009,** *9* (3), 1212-1216.
36. Kidd, B. E.; Forbey, S. J.; Steuber, F. W.; Moore, R. B.; Madsen, L. A., Multiscale Lithium and Counterion Transport in an Electrospun Polymer-Gel Electrolyte. *Macromolecules* **2015,** *48* (13), 4481-4490.
37. Hou, J.; Li, J.; Mountz, D.; Hull, M.; Madsen, L. A., Correlating morphology, proton conductivity, and water transport in polyelectrolyte-fluoropolymer blend membranes. *Journal of Membrane Science* **2013,** *448*, 292-299.
38. Gilbert, J. B.; Luo, M.; Shelton, C. K.; Rubner, M. F.; Cohen, R. E.; Epps, T. H., III, Determination of Lithium-ion Distributions in Nanostructured Block Polymer Electrolyte Thin Films by X-ray Photoelectron Spectroscopy Depth Profiling. *ACS Nano* **2015,** *9* (1), 512-520.
39. Gartner, T. E.; Morris, M. A.; Shelton, C. K.; Dura, J. A.; Epps, T. H., III, Quantifying Lithium Salt and Polymer Density Distributions in Nanostructured Ion-Conducting Block Polymers. *Macromolecules* **2018,** *51* (5), 1917-1926.
40. Kuan, W.-F.; Reed, E. H.; Nguyen, N. A.; Mackay, M. E.; Epps, T. H., III, Using tapered interfaces to manipulate nanoscale morphologies in ion-doped block polymers. *MRS Communications* **2015,** *5* (2), 251-256.
41. Stafford, C. M.; Roskov, K. E.; Epps, T. H., III; Fasolka, M. J., Generating thickness gradients of thin polymer films via flow coating. *Review of Scientific Instruments* **2006,** *77* (2), 023908.
42. Dura, J. A.; Pierce, D. J.; Majkrzak, C. F.; Maliszewskyj, N. C.; McGillivray, D. J.; Lösche, M.; O'Donovan, K. V.; Mihailescu, M.; Perez-Salas, U.; Worcester, D. L.; White, S. H., AND/R: Advanced neutron diffractometer/reflectometer for investigation of thin films and multilayers for the life sciences. *Review of Scientific Instruments* **2006,** *77* (7), 074301.
43. Maranville, B.; Ratcliff, W., II; Kienzle, P., reductus: a stateless Python data reduction service with a browser front end. *Journal of Applied Crystallography* **2018,** *51* (5), 1500-1506.
44. Kienzle, P. A.; Maranville, B. B.; O'Donovan, K. V.; Ankner, J. F.; Berk, N. F.; Majkrzak, C. F. https://www.nist.gov/ncnr/reflectometry-software. (accessed 11/15/2018).
45. Bielecki, A.; Burum, D. P., Temperature Dependence of ^{207}Pb MAS Spectra of Solid Lead Nitrate. An Accurate, Sensitive Thermometer for Variable-Temperature MAS. *Journal of Magnetic Resonance, Series A* **1995,** *116* (2), 215-220.
46. Young, W. S.; Albert, J. N. L.; Schantz, A. B.; Epps, T. H., III, Mixed-Salt Effects on the Ionic Conductivity of Lithium-Doped PEO-Containing Block Copolymers. *Macromolecules* **2011,** *44* (20), 8116-8123.
47. Sears, V. F., Neutron scattering lengths and cross sections. *Neutron News* **1992,** *3* (3), 26-37.
48. Liu, G.; Stoykovich, M. P.; Ji, S.; Stuen, K. O.; Craig, G. S. W.; Nealey, P. F., Phase Behavior and Dimensional Scaling of Symmetric Block Copolymer−Homopolymer Ternary Blends in Thin Films. *Macromolecules* **2009,** *42* (8), 3063-3072.
49. Luo, M.; Brown, J. R.; Remy, R. A.; Scott, D. M.; Mackay, M. E.; Hall, L. M.; Epps, T. H., III, Determination of Interfacial Mixing in Tapered Block Polymer Thin Films: Experimental and Theoretical Investigations. *Macromolecules* **2016,** *49* (14), 5213-5222.

50. Anastasiadis, S. H.; Russell, T. P.; Satija, S. K.; Majkrzak, C. F., The morphology of symmetric diblock copolymers as revealed by neutron reflectivity. *The Journal of Chemical Physics* **1990,** *92* (9), 5677-5691.
51. Fox, T. G. J.; Flory, P. J., Second-Order Transition Temperatures and Related Properties of Polystyrene. I. Influence of Molecular Weight. *Journal of Applied Physics* **1950,** *21* (6), 581-591.
52. Kuan, W.-F.; Remy, R.; Mackay, M. E.; Epps, T. H., III, Controlled ionic conductivity via tapered block polymer electrolytes. *RSC Advances* **2015,** *5* (17), 12597-12604.
53. Abbrent, S.; Greenbaum, S., Recent progress in NMR spectroscopy of polymer electrolytes for lithium batteries. *Current Opinion in Colloid & Interface Science* **2013,** *18* (3), 228-244.
54. Oza, Y. V.; MacFarlane, D. R.; Forsyth, M.; O'Dell, L. A., Unexpected effect of tetraglyme plasticizer on lithium ion dynamics in PAMPS based ionomers. *Physical Chemistry Chemical Physics* **2016,** *18* (28), 19011-19019.
55. Yuan, R.; Teran, A. A.; Gurevitch, I.; Mullin, S. A.; Wanakule, N. S.; Balsara, N. P., Ionic Conductivity of Low Molecular Weight Block Copolymer Electrolytes. *Macromolecules* **2013,** *46* (3), 914-921.
56. Ballard, D. G. H.; Wignall, G. D.; Schelten, J., Measurement of molecular dimensions of polystyrene chains in the bulk polymer by low angle neutron diffraction. *European Polymer Journal* **1973,** *9* (9), 965-969.
57. Morèse-Séguéla, B.; St-Jacques, M.; Renaud, J. M.; Prod'homme, J., Microphase Separation in Low Molecular Weight Styrene-Isoprene Diblock Copolymers Studied by DSC and 13C NMR. *Macromolecules* **1980,** *13* (1), 100-106.